GEOLOGICA CARPATHICA, DECEMBER 2018, 69, 6, 515–527 doi: 10.1515/geoca-2018-0030

Multiphase carbonate cementation in the Miocene Pétervására Sandstone (North Hungary): implications for basinal fluid flow and burial history

EMESE SZŐCS✉ and KINGA HIPS

MTA–ELTE Geological Geophysical and Space Science Research Group, 1117 Budapest, Pázmány sétány 1/C, Hungary;
✉meseszocs@gmail.com

(Manuscript received June 10, 2018; accepted in revised form November 28, 2018)

Abstract: The paper focuses on the reservoir heterogeneity of a sandstone formation in which the main issue is the evaluation of diagenetic features. Integrated data from field observations as well as petrographic and geochemical analyses from surface and core sections from different structural settings were applied. In the shallow marine Pétervására Sandstone, eogenetic minerals are comprised of calcite, pyrite and siderite; mesogenetic minerals are albite, ankerite, calcite, quartz, mixed layer clays and kaolinite. Dissolution occurred during mesogenetic and telogenetic phases. Ankerite is only present in the core setting, where the sandstone is at ca. 900 m depth and diagenetic calcite predates quartz cementation. Based on stable isotopic values ($\delta^{13}C_{V\text{-}PDB}$ −18.3 to −11.4 ‰ and $\delta^{18}O_{V\text{-}PDB}$ −9.5 to −7.2 ‰), diagenetic calcite is of mesogenetic origin and was precipitated from fluids migrated along fault zones from the underlying, organic matter-rich formation. In outcrop setting, on the other hand, calcite is present in a larger quantity and postdates quartz cementation. Carbon isotope data ($\delta^{13}C_{V\text{-}PDB}$=−9.9 to −5.1 ‰) indicate less contribution of light isotope, whereas more negative oxygen isotopic values ($O_{V\text{-}PDB}$=−13.1 to −9.9 ‰) likely imply higher temperature of mesogenetic fluids. However, carbon–oxygen isotope covariation can indicate precipitation from meteoric fluid. In this case, further analyses are required to delineate the final model.

Keywords: calcite, diagenesis, sandstone petrography, stable isotopes, fluid flow, lower Miocene.

Introduction

Studies of reservoir analogue sections provide useful data for subsurface reservoir modelling. In the case of clastic deposits, the depositional facies is commonly the major control on reservoir architecture, but diagenetic cementation can be an effective modifying factor. Carbonate cement in sandstones plays a substantial role in reservoir quality evolution (e.g., Morad 1998; El-ghali et al. 2006; Gier et al. 2008; Karim et al. 2010; Oluwadebi et al. 2018). Concretionary calcite cementation of various origins was reported from numerous sandstone formations (e.g., McBride et al. 1994; El-ghali et al. 2006; Van Den Bril & Swennen 2008; Wanas 2008; Bojanowski et al. 2014). Other diagenetic carbonates, such as siderite (Mozley 1989; Pye et al. 1990; Baker et al. 1995; Makeen et al. 2016) and ankerite or ferroan dolomite (Hendry et al. 2000; Hendry 2002; Lima & De Ros 2002), can also influence the reservoir quality. Diagenetic carbonate minerals provide data about the burial history and chemistry of diagenetic fluids.

In this study, diagenetic features of the early Miocene Pétervására Sandstone are presented. This formation is a hydrocarbon reservoir rock in the central part of Hungary, whereas in the northern part only traces of bitumen occur (Lakatos et al. 1991; Kázmér 2004). Sztanó (1994) described and interpreted the sedimentary geometries within the siliciclastic succession deposited in tide-dominated shallow water. This paper documents the results of petrographic and geochemical analysis in core and outcrop samples; based on these data the burial history was reconstructed. The correlation of the studied sections revealed the spatial variability of diagenetic processes, especially calcite cementation and its contribution to the heterogeneity of the reservoir rocks.

Geologic setting

The Pétervására Sandstone Formation can be found in the northern part of Hungary and the southern part of Slovakia; it covers an area of 1500 km^2 (Fig. 1). It consists of medium to coarse-grained, cross-stratified glauconitic sandstone punctuated by conglomerate beds and fine-grained, thick-bedded to massive sandstone (Sztanó 1994). The thickness of the formation is 200–600 m.

In the Oligocene, the Paratethys Basin (a large inland sea) formed in the Alpine–Carpathian depositional area (Báldi 1983; Rögl & Steininger 1983). This basin was made up of a chain of basins with varying structural developments. The Pétervására Sandstone was formed in the North Hungarian Bay, an embayment of the Paratethys, where tide-influenced deposition began in the Early Miocene (Eggenburgian). This bay was connected to the Paratethys through the Eastern Slovakian Seaway (Sztanó & Boer 1995). The Late Oligocene–Early Miocene deep marine siltstone formation is overlain by shallow marine sandstone that reflects a shallowing-upward trend

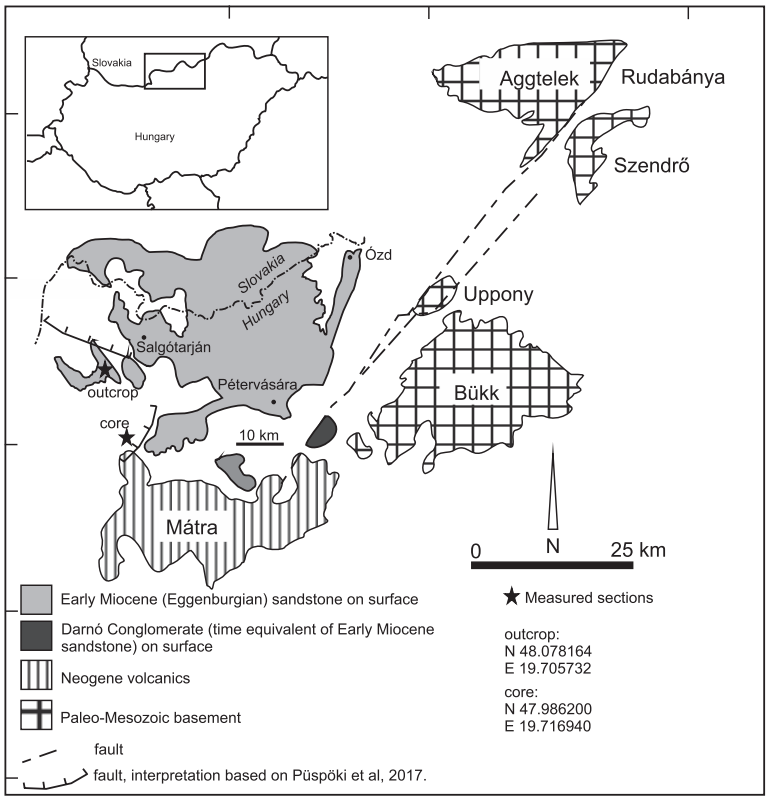

Fig. 1. Location of the study area. Surface distribution map of the Pétervására Sandstone Formation (Sztanó 1994) and geologic map of the area (Márton & Fodor 1995) showing locations of the studied outcrop and a core section.

(Báldi & Báldi-Beke 1985). The Eocene–Lower Miocene sedimentary sequence ends with non-marine deposits followed by a 25-m-thick coal formation (Báldi & Báldi-Beke 1985; Sztanó & Tari 1993).

The Pétervására Sandstone is composed of four shore-parallel facies units (Sztanó & Tari 1993), which were formed in gradually shallower water depth from offshore to onshore from base to top. These are the following: 1) fine, rippled, silty sand, the transition toward the time-equivalent Szécsény Slier; 2) fine to medium-grained sandstone with decimetre-scale cross-bedding; 3) medium to coarse-grained sandstone, characterized by large-scale cross-bedding with sets up to 10 m in height; 4) conglomerate lobes of 1.5–3 m height. The influence of tidal motions is the most evident in facies units deposited in shallow water. In the decimetre-scale cross-bedded sandstone, the foresets are covered by mud drapes. The sandy material was derived from the south, whereas coarse-grained sand to pebble-sized components have the same source area as the coeval Darnó Conglomerate (Sztanó & Józsa 1996). The latter formation is located near the Darnó Fault and its components were derived from the Meliata–Szarvaskő Nappe of the Bükk Unit, which consists of Triassic–Jurassic ocean-floor basalt and radiolarite.

Sandstone was studied in outcrop and core sections, located in various structural settings (Fig. 2). At Kishartyán, the sandstone crops out in a 32 m-high and 300 m-long section (Fig. 2B). This section exhibits an coarsening-upward and thickening sandstone superposed by conglomerate beds (Sztanó 1994). A petrographic and diagenetic study of the outcrop at Kishartyán was provided by Szőcs et al. (2015).

In the core section (Sámsonháza 16; Sh-16/a), the studied sandstone occurs from 842 to 1009 m (below surface) where fine to coarse-grained sandstone is intercalated by conglomerate beds (Fig. 2A).

According to hydrogeologic studies, two distinct hydrologic systems were detected in the subsurface basinal deposits of the study area: (1) an upper, gravity-driven meteoric water flow and (2) a lower, compaction-driven brine water flow (Tóth & Almasi 2001; Horváth et al. 2015). Based on pore-water data, the same systems are recognisable in the studied core section. The pore-water in sandstone (analysed at 890 m depth) is of the Na-HCO_3-Cl type with 3104 mg/l total dissolved solids (TDS) at 37 ˚C with 2.4 bar pressure (Hámor 1985). This indicates meteoric water recharge into the porous formation and it indicates a normal geothermal gradient. On the other hand, in the underlying siltstone at 1150 m, which has much lower porosity than the sandstone, the pore-water temperature is 68 ˚C. This latter temperature indicates a much higher geothermal gradient that is due to the elevated heat flow which affected the basinal deposits during the Miocene–Pliocene synrift phase (Horváth et al. 2015).

Hydrocarbon system of the North Hungarian Palaeogene Basin

Palaeogene formations in the Pannonian Basin are considered to be a significant hydrocarbon system (Horváth & Tari 1999). In this system the most active source rocks are the Upper Eocene and Lower Oligocene Tard Clay and the Lower Oligocene Kiscell Clay, with average TOC values of 0.5–1 wt. % which locally rise up to 4.5 wt. % (Milota et al. 1995; Badics & Vető 2012). Maturation has likely occurred in the Late Miocene and/or Pliocene during maximal heat flow (Milota et al. 1995). The most effective traps are structural, stratigraphic and combination ones. Oligocene turbidite and the studied sandstone formation are the reservoir rocks of this hydrocarbon system.

In the eastern part of the basin, near the study area, a few hydrocarbon exploration wells encountered oil shows (Kázmér 2004). The equivalent unit of the studied sandstone is a reservoir rock in the Gödöllő–Tóalmás–Tura–Jászberény area, but the reservoir intervals of wells were not cored (Lakatos et al. 1991).

Methods

Thirty-two sandstone samples were collected from the outcrop at Kishartyán (Fig. 2B) by hammer and by drilling horizontally from the rock surface to 30 cm depth with 3 and 5-cm-diametre cores (Fig. 2C,D). The samples were collected along vertical and horizontal sections. Five sandstone samples from the core section of the borehole Sámsonháza 16 (Sh-16/a) were collected from the depth interval of 840 to 1000 m (Fig. 2A). Samples from outcrop and borehole represents the following facies unit of the Pétervására Sandstone: 2) fine to medium-grained sandstone with decimetre-scale cross-bedding; 3) medium to coarse-grained sandstone, characterized by large-scale cross-bedding with sets up to 10 m in height (cf. Sztanó 1994). Samples were impregnated in blue epoxy under vacuum and 30 µm-thick thin sections were prepared. Thin sections were stained with Alizarin Red S and K-ferricyanide as described by Dickson (1966) in order to determine carbonate minerals. They were examined by conventional microscopic petrographic methods. Point counting was performed on 18 samples to investigate quantitative composition and pore volume. In each sample, 350 points were counted. Cathodoluminescence (CL) studies were performed using a MAAS-Nuclide ELM-3 cold-cathode CL device on polished thin sections. A microscope equipped with an Hg vapour lamp and filters for blue light excitation (450–490 nm) was used to detect organic matter in the samples. The filter set was composed of a diachromatic beam splitter (510 nm) and a barrier filter (515 nm).

X-ray diffraction analysis of <2 µm fractions was carried out using a Siemens D 5000-type diffractometer (CuKα). The sandstone was crushed and treated with 10 % C_2H_4O solution and then washed with distilled water. Oriented XRD mounts were prepared by pipetting the clay suspension onto glass slides and were analysed after air-drying and after vapour saturation with ethylene glycol at 60 °C for 12 hours. An Amray 1830i-type Scanning Electron Microscope equipped with INCA Energy-dispersive X-ray spectrometer was used in the secondary electron (SE), backscatter electron (BE) and cathodoluminescent (CL) modes on polished thin sections and in broken surfaces. The chemical composition of minerals was established with JXA-8530F-type Electron Probe Microanalyses. Stable carbon and oxygen isotopic analyses were carried out by a Finnigan MAT delta S-type mass spectrometer after samples being pulverized and using a conventional anhydrous phosphoric acid digestion method under vacuum. The results are expressed in δ-notation on the Vienna PDB standard.

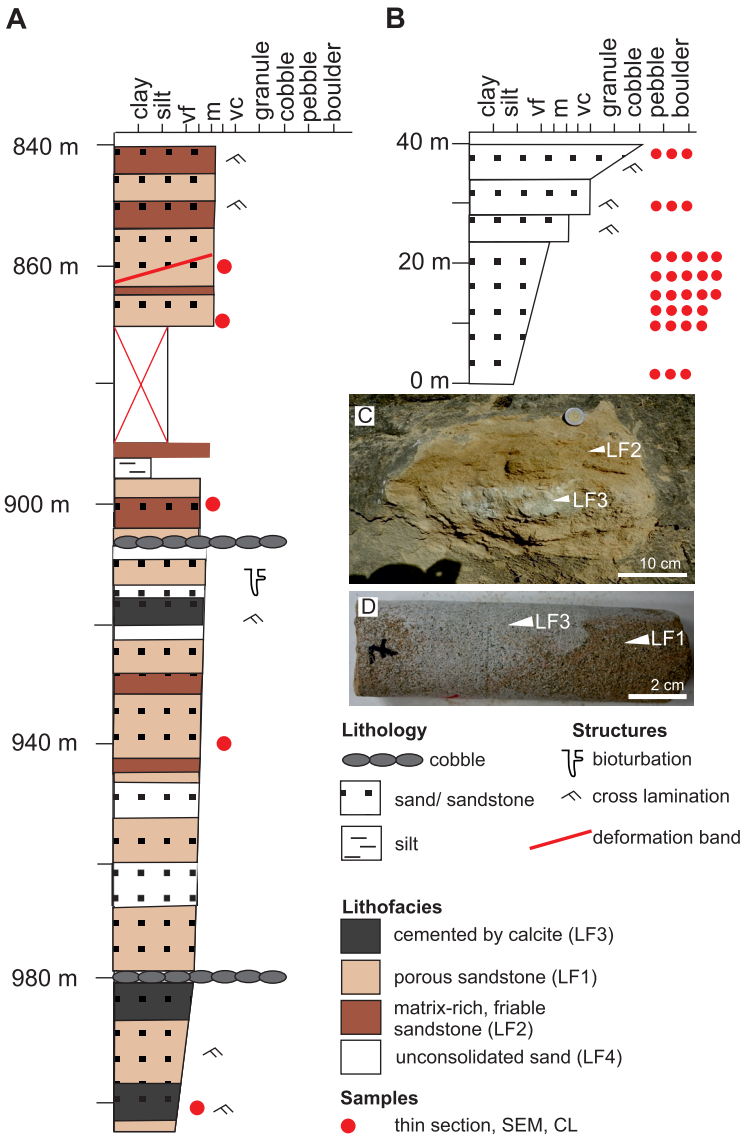

Fig 2. A — Lithology of the core section Sh-16/a. Only three calcite-cemented beds (LF3) are present. **B** — Lithology in the outcrop section at Kishartyán. Due to high variability, lithofacies distribution is not marked here. **C, D** — Distribution of lithofacies in outcrop samples.

Results

Sandstone petrography of detrital grains

The studied intervals consist of fine to very coarse-grained sandstone, in which sorting ranges from moderate to well, with angular to well-rounded detrital grains. The sandstone is classified as litharenite and feldspathic litharenite, with the average framework of $Q_{43}F_{11}L_{46}$ (outcrop samples) and $Q_{42}F_7L_{49}$ (core samples; Fig. 3) according to the Folk (1974) classification.

Quartz is the most abundant detrital mineral. Monocrystalline quartz usually exhibits straight, occasionally sweeping extinction. Polycrystalline quartz is slightly less abundant than monocrystalline quartz. Chert and radiolarite fragments are

also common, and these are generally more rounded than quartz grains. The total amount of quartz and chert varies between 23 and 43 %. The total feldspar content is around 5 % in core samples and 7 % in outcrop ones. K-feldspar is often associated with kaolinite and is more abundant than plagioclase.

The amount of metamorphic lithic fragments ranges between 11 and 39 %. They are composed of micaschists with muscovite, quartz, chlorite, gneiss, and quartzite. Plutonic rock fragments (granitoids, microdiorites), volcanic and ophiolitic ones are also common (average 7 %). Detrital dolomite averages 5 % (outcrop samples) and 11 % (core samples). Limestone fragments and bioclasts are scarce. Muscovite, chloritized biotite, glauconite group minerals, and fragments of metamorphic minerals such as garnet, rutile, and staurolite, are also present. The matrix content of sandstone can reach 25 %. However, some of the samples are totally matrix-free. Pseudomatrix represented by mica and clay-rich rock fragments is also present.

Lithofacies types and distribution

Based on point counting and microscope observations, three main lithofacies types were distinguished. Porous sandstone (LF1) with porosites of 10–25 % is the most common one in the outcrop as well as in the core (Fig. 4A). Matrix-rich sandstone (LF2) has high detrital and diagenetic clay mineral content and includes clay laminae located between the foresets (Fig 4B). Cement-rich sandstone (LF3) has porosity lower than 10 % and calcite content is between 12 and 27 % (Fig. 4C). Sandstone in these lithofacies can be classified as graywacke. In addition, in the core section a semi-consolidated sand was classified as LF4. This lithofacies was not analysed in this study. The spatial distribution of these lihofacies is irregular in the outcrop, and gradual transitions are observed in both outcrop and core sections (Fig. 2C, D). Both in core and outcrop sections the porous sandstone (LF1) is the predominant lithofacies, whereas matrix-rich sandstone (LF2) is subordinate. The cement-rich sandstone (LF3) is relatively widespread in the outcrop section. In the core, three calcite-cemented layers with a thickness of 10 cm can be found in the lower part of the section (Fig. 2A).

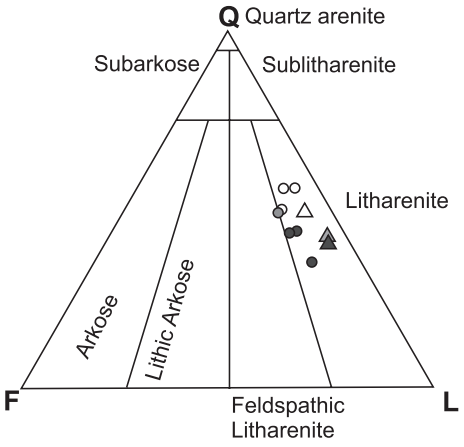

Fig. 3. Ternary diagram for the detrital components. Q=quartz, F=feldspar, L=lithoclasts/rock fragments after Folk (1974).

Petrography of diagenetic components

Deformation of ductile grains such as mica, glauconite and lithoclasts are common in both studied sections. In calcite-free intervals (LF1, LF2) of core section, linear contacts are observed and selective fracturing of rigid grains such as dolomite, quartz and feldspar also occurs (Fig. 4A). In calcite-cemented sandstone (LF3) of core section, point contacts are dominant. In outcrop section (LF1, LF2, LF3), linear or concavo-convex grain contacts are more abundant than point contacts; in addition, microstylolite is also encountered (Fig. 4C). Accordingly, the grade of compaction is low to moderate in calcite cemented sandstone (LF3) of core section and high in every other lithofacies.

The observed diagenetic minerals are various carbonates, quartz, albite, K-feldspar, kaolinite, mixed-layer illite/smectite, framboidal pyrite and glauconite. Pyrite occurs as fine framboidal crystals (<2 μm). The pyrite crystals are scattered around mottles of clay minerals or mica, or engulfed by coarse carbonate crystals. Glauconite is present as peloids and pore-filling of bioclasts. The latter case suggests diagenetic origin. Diagenetic albite is present as a replacive phase in

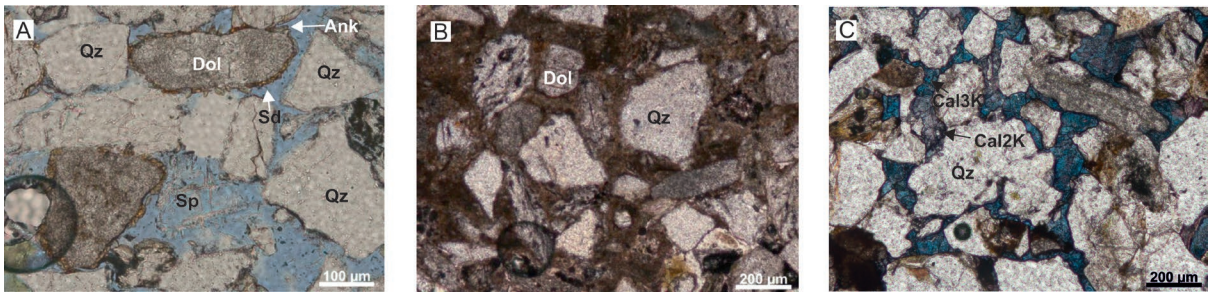

Fig. 4. Photomicrographs (PPL) of sandstone from various lithofacies. **A** — Porous sandstone (LF1) with abundant inter-granular and secondary skeletal pores (thin section impregnated with blue-dye epoxy). Pre-compactional grain-rimming siderite cement around dolomite grains is present. **B** — Matrix-rich sandstone (LF2) where authigenic siderite is scattered in matrix. **C** — Tightly-cemented sandstone (LF3). Post-compactional blue-stained, iron-bearing replacive (Cal2K) and cement calcite (Cal3K) is ubiquitous (thin section stained by Dickson solution). (A, B samples from core, C sample from outcrop.) Dol=dolomite, Fsp=feldspar, Qz=detrital quartz, Sd=siderite, Sp=secondary porosity.

detrital K-feldspar grains along fractures or as euhedral overgrowth cement. These are non-luminescent and have a chemically pure albite composition (Fig. 5A,B). K-feldspar overgrowth cement appears in porous sandstone (LF1) as thin, non-luminescent rims and it is present only in those sides of detrital grains which are not in contact with other grains (Fig. 5C). Both diagenetic albite and K-feldspar are common in the outcrop samples, whereas these minerals are scarce or totally missing in the core section. Small quantities of quartz overgrowth cement can be found in calcite-cement free (LF1) intervals of the core section and both in calcite-cemented (LF3) and calcite cement-free (LF1, LF3) intervals of the outcrop (Fig. 5D). Kaolinite is the most common clay mineral. The pore-filling kaolinite, in the largest quantity, appears as well-developed blocky and vermicular crystals of several tens of microns (Fig. 5D,E). Kaolinite associated with detrital muscovite is also abundant and it is localised between 001 surfaces that had been separated by expansion (Fig. 5F). In the intragranular and compaction-reduced intergranular pores, along with abundant microporosity a limited quantity of small blocky kaolinite crystals is attached to the surface of plagioclase grains (Fig. 5G). Kaolinite can be found in calcite cement-free intervals (LF1) of the core section and in every lithofacies of the outcrop section. Other clay minerals in the outcrop and the core section consist of mixed layer illite-smectite (I/S), smectite, illite and chlorite (Fig. 5H,I).

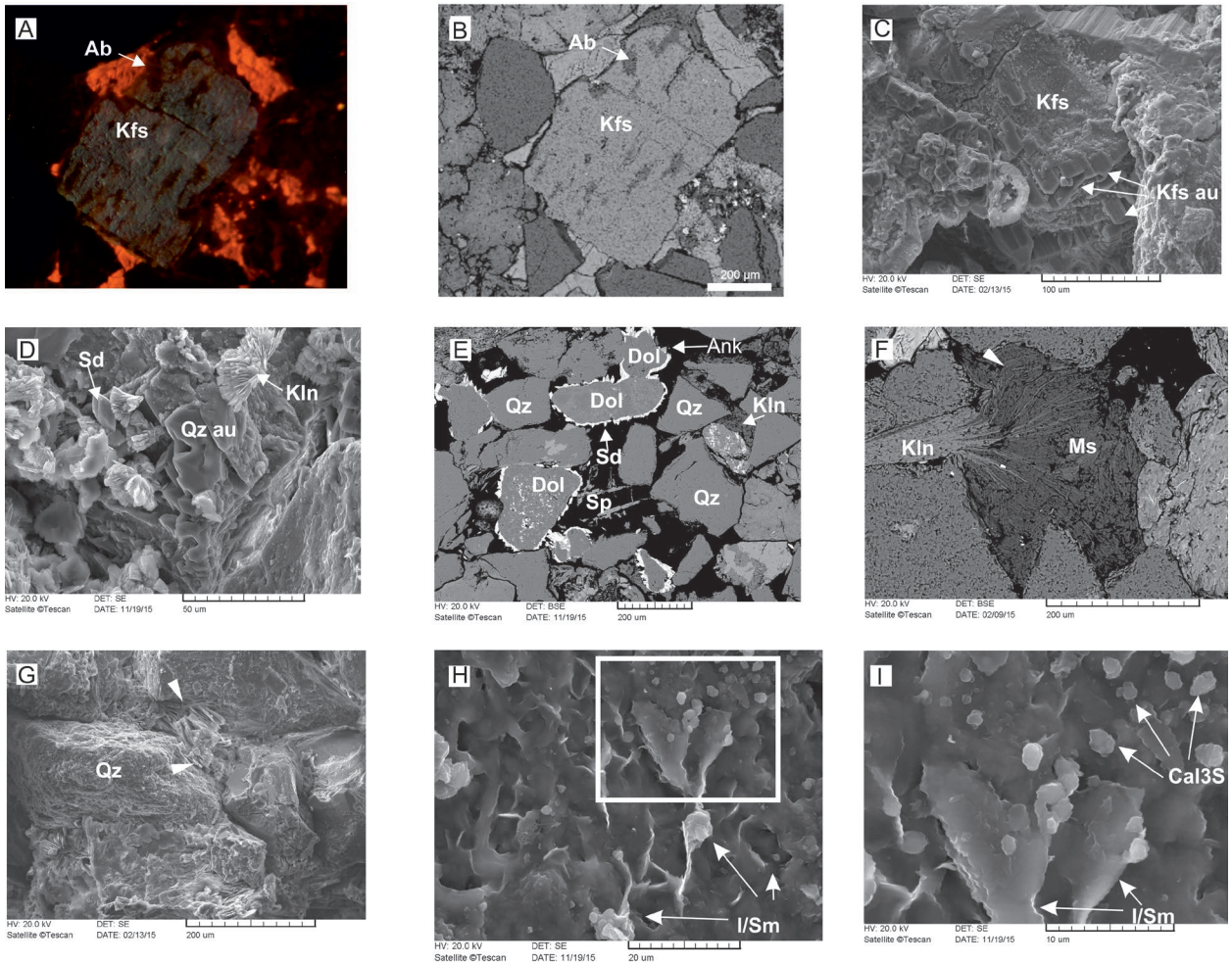

Fig. 5. Diagenetic minerals. **A, B** — Replacive non-luminescent albite in mottles of light-blue luminescent detrital K-feldspar. The majority of detrital grains are non-luminescent, whereas pore-occluding and replacive calcite exhibit bright orange luminescent colour. (A: CL image and B: BSE image, sample from outcrop). **C** — Detrital K-feldspar grain with post-compactional overgrowth cement (SE image, sample from outcrop). **D** — Quartz cement (Qo), diagenetic vermicular kaolinite (Kln), and siderite cement (Sd) in open pore space (SE image, sample from borehole). **E** — Siderite cement exhibits flattened rhombohedral shape around dolomite grains. Siderite is partially replaced by ankerite (arrow). Secondary skeletal porosity is formed by dissolution of K-feldspar grains whereas pore-reducing kaolinite cement is also present (BSE image, sample from core). **F** — Diagenetic, pore-filling kaolinite (Kln) localised between 001 surfaces of detrital mica (Ms), separating them by expansion (BSE image, sample from outcrop). **G** — Pore-filling kaolinite booklets (arrows) which overlap the linear contact of quartz grains (Q) (SEM–SE, sample from outcrop). **H** — Mixed-layer grain-coating smectite-illite. **I** — Showing a detail of H in higher magnification where mixed-layer clays are covered by calcite plates of micron size (Cal3S) (SEM–SE, sample from core). Abbreviations: Ab=albite, Ank=ankerite, Dol=dolomite, I/Sm=mixed layer illite-smectite, Kfs=K-feldspar, Kfs au=authigenic K-feldspar, Kln=kaolinite, Ms=muskovite, Qz=detrital quartz, Qzau=quartz overgrowth cement, Sd=siderite, Sp=secondary porosity.

Diagenetic carbonate minerals

Carbonate minerals, including siderite, ferroan dolomite/ankerite, ferroan and non-ferroan calcite, are present in both studied sections. In outcrop samples these minerals are present in a higher amount, but in lower variability than in samples from core. Calcite is the volumetrically most abundant diagenetic mineral phase, varying between 0 and 25 %. The proportion of siderite and ferroan dolomite/ankerite is less than 5 %. In the outcrop, calcite-cemented lenses appear in every 30–50 cm interval and they also form continuous cemented layers. In the core, calcite cement is encountered only in a few layers, which are less than 10 cm in thickness. Ferroan dolomite/ankerite is only present in the core section. The petrographic features of diagenetic carbonates are different in the outcrop and in the core; therefore, they are described separately.

Core section

The majority of diagenetic carbonate minerals are equally distributed in every lithofacies. Calcite phases (Cal1S, Cal2S) are only present in cement-rich sandstone (LF3), while tiny crystal plates (Cal3S) are confined to LF1 and LF2. Siderite crystals exhibit small, flattened rhombs (10–30 μm). They are commonly associated with detrital dolomite grains as grain-rimming cement (Figs. 5E; 6A,B,C). Locally they are also scattered in the matrix. Siderite ranges from 1 to 6 %, and is non-luminescent.

A thin alteration rim on dolomite grains exhibits bright orange luminescence colour and is slightly enriched in Fe (Fig. 6B). Ferroan dolomite/ankerite (*sensu* Nickel & Grice, 1998) is present in small quantity (<5 %). The detrital dolomite as well as the siderite cement are partially replaced by anhedral crystals of ferroan dolomite/ankerite that can achieve several tens of microns in size (Fig. 6B,C). They are non-luminescent, and are characterized by mottled BSE image. These crystals include remnants of siderite of small size. In porous-sandstone (LF1), ankerite is rarely present within detrital dolomite grains, as irregular mottles arranged in the network (Fig. 5E) or as vertical hairline veins (Fig. 6C). In cement-rich sandstone (LF3) the amount of siderite is lower than in porous sandstone.

Calcite-cemented sandstone (LF3) is present only in the lower part of the section. Calcite (Cal1S and Cal2S) occurs as a pore-occluding phase in the form of mosaic spar or microspar crystals (Fig. 6D,E). In the porous sandstone (LF1), on the other hand, calcite occurs as micron-sized plates (Cal3S), which cover the surface of smectite and smectite/illite (Fig. 5H,I).

In calcite-cemented sandstone, the cement crystals commonly exhibit two zones. The first one (Cal1S) stains pink and shows bright orange luminescence colour (Fig. 6D,E). On the other hand, the second zone (Cal2S) stains blue and shows dull red luminescence (Fig. 6D,E). The calcite crystals also replace detrital dolomite grains and diagenetic minerals, such as siderite and ferroan dolomite/ankerite (Fig. 6B). The calcite cement surface is occasionally covered by residual organic matter.

Outcrop section

Pseudomorph of flattened rhombohedral crystals composed of iron oxides are present around dolomite grains and scattered in the matrix. These crystals show voluminous microporosity and, as the crystal shape suggests, they were formed via alteration of siderite. Calcite is present exclusively in the calcite-cemented sandstone lithofacies (LF3). The crystals exhibit various petrographic characters and occur as replacive and cement phases. Calcite spars, which occlude the intergranular pore space where the framework grains have mainly point contacts, have a very thin, non-luminescent first growth band (Cal1K). This zone occurs as an uneven rim around grains. In other cases, calcite crystals (Cal2K, Cal3K) commonly engulf detrital grains having linear contacts or microstylolitic surfaces (Fig. 6F,G,H,I). The replacive calcite (Cal2K) stains mauve to blue and exhibits mottled to dull red luminescence colour (Fig. 6F,G). The cement phase (Cal3K), which occurs in compaction-reduced intergranular pore space and as a second growth band of mosaic crystals following Cal1K, exhibits growth zonation via mauve and blue staining and bright orange and dull red luminescence colour (Fig. 6F,G).

The replacive calcite (Cal2K) occurs as either mosaic crystals (and among them, the remnants of various minerals can be commonly found), or as poikilotopic crystals which include remnants of detrital and diagenetic minerals (Fig. 6H). These remnants are detrital plagioclase, K-feldspar, quartz, dolomite, rock fragments of magmatic and volcanic origin, as well as diagenetic minerals, such as altered siderite (Fig. 6I). The size and shape of the mosaic crystal sets, as well as of the poikilotopic crystals among the framework grains, are similar to detrital grains (Fig. 6G,H).

Porosity

Intergranular porosity, modified by compaction and minor cement precipitation, is observed in LF1 (Fig. 7A). Secondary intragranular porosity is associated with detrital K-feldspar and plagioclase (Fig. 7B,C). In addition, very small remnants of feldspar and scattered flattened rhombohedral cement occur in oversized pores, suggesting secondary pore formation via enlargements of the primary one (Fig. 7A). In the outcrop samples, the intragranular dissolution pores are cemented by kaolinite (Fig. 7B) or calcite (Fig. 6I). In the core samples, these pores are open and the partially dissolved feldspar grains are engulfed by calcite (Fig. 7C). The porosity of the studied sandstone ranges from <1 % to 25 %. In the porous sandstone from the outcrop, the average value of the modified intergranular porosity is 13 %, whereas intragranular porosity is around 3.5 %. These values are 7 % and 2 % in the core. In calcite-cemented sandstone (LF3) and matrix-rich sandstone (LF2), the total value of porosity is generally below 5 %, and it is slightly lower in the core than in the outcrop.

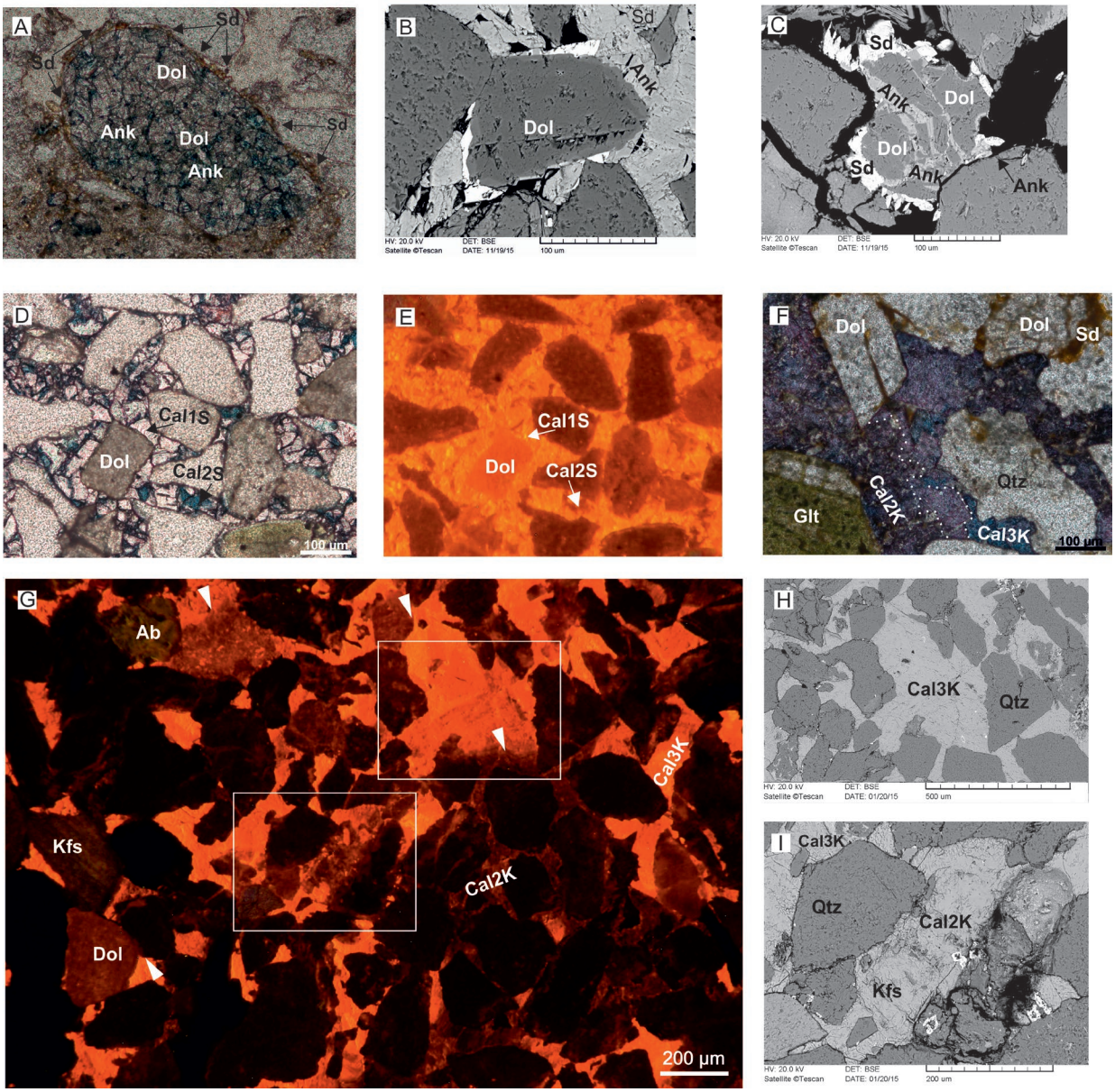

Fig. 6. Diagenetic carbonate minerals. **A** — Detrital dolomite grain is partially replaced by ankerite along irregular network (stained blue) and it is surrounded by siderite cement (optical photomicrograph; sample from core). **B** — Detrital dolomite with ferroan alteration rim. Siderite cement and replacive ankerite crystals are partially replaced by calcite (SEM–BSE image from core). **C** — Detrital dolomite grain, with grain-rimming siderite cement, fractured and partially replaced by ankerite (SEM–BSE sample from core). **D, E** — Grain-rimming calcite cement stained pink and exhibiting bright orange luminescent colour (Cal1S) is post-dated by calcite cement stained blue and exhibiting dull red luminescent colour. (Optical photomicrograph and CL, sample from core). **F** — Purple-stained replacive calcite (Cal2K, delineated by dotted line) with scattered, tiny remnants of brownish precursor minerals. The first phase of cement crystals (Cal2K) has a straight crystal face (dotted line), whereas the second phase (Cal3K) fills the pore space. (Optical photomicrograph, sample from outcrop.) **G** — Calcite, replacive and cement crystals, among the framework detrital grains exhibit two generations: dull red luminescent colour calcite (Cal2K) and a second zone of cement crystals of bright orange luminescent colour (Cal3K) (CL, sample from outcrop). **H, I** — Details of (G) in SEM-BSE. Replacive calcite contains no (H) or few (I) remnants of detrital grains. Secondary, enlarged intergranular and intragranular porosity suggest a dissolution event (SEM–BSE sample from core). Ab=albite, Ank=ankerite, Dol=dolomite, Glt=glauconite, Kfs=K-feldspar, Kln=kaolinite, Qz=detrital quartz, Sd=siderite.

Carbon and oxygen isotopic composition of calcite

Due to the small size and close petrographic association of calcite phases, their separate measurement was not possible. The tiny size of Cal3S did not allow the measurement of this phase. The isotopic values of the calcite from the core represent a bulk composition of Cal1S and Cal2S. Cal1K is only present in a very small quantity, so the isotopic values of outcrop calcite represent a bulk composition of Cal2K and Cal3K. The $\delta^{13}C_{V\text{-}PDB}$ values for calcite in the core vary from −18.3 to

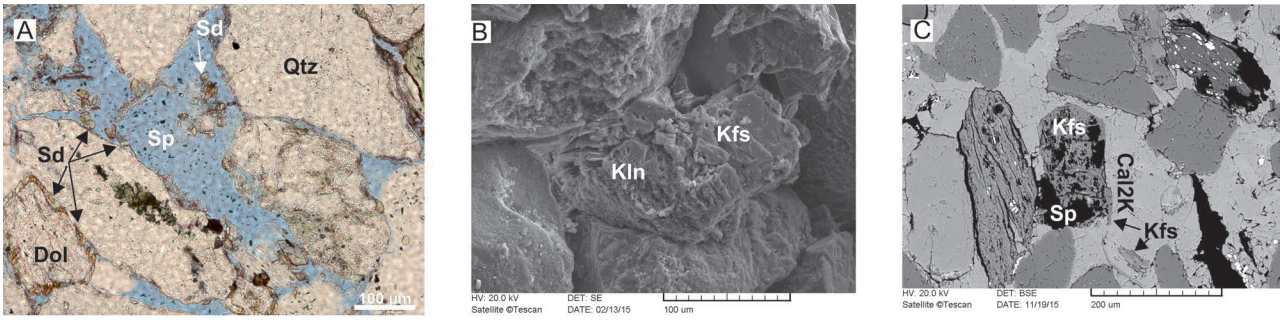

Fig. 7. Porosity types in sandstone. **A** — Skeletal and enlarged intergranular porosity. The dissolved grain was likely dolomite, indicated by remnants of siderite crystals (optical photomicrograph, sample from core). **B** — Secondary porosity and microporous kaolinite inside a detrital feldspar grain (SEM–BSE, sample from outcrop.). **C** — Open secondary porosity within euhedral albite. The grain is surrounded by diagenetic calcite (Cal2K) which indicates that the feldspar dissolution post-dated the calcite cementation (SEM–BSE, sample from core). Dol=dolomite, Kfs=K-feldspar, Kln=kaolinite, Qz=detrital quartz, Sd=siderite, Sp=secondary porosity.

−11.4 ‰, whereas the $\delta^{18}O_{V\text{-}PDB}$ values range between −9.5 and −7.2 ‰. Calcite in the outcrop yielded $\delta^{13}C_{V\text{-}PDB}$ values ranging from −9.9 to −5.1 ‰ and $\delta^{18}O_{V\text{-}PDB}$ values of −13.1 to −9.9 ‰, respectively (Fig. 8).

Geochemical composition of carbonate minerals

The chemical composition of diagenetic carbonates shows slight or moderate variations. Siderite is relatively rich in $MgCO_3$ (4.2–18.7 %) and $CaCO_3$ (7–12 %) and poor in $MnCO_3$ (0.3–1.3 %), whereas $FeCO_3$ content varies between 68.5 and 81.9 %. In ankerite/ferroan dolomite crystals, the $FeCO_3/MgCO_3$ proportion commonly decreases from core to edge, varying between 0 and 1.4. The $MnCO_3$ content is below 0.6 %. The bright orange luminescent alteration rim of detrital dolomite grains is enriched in iron compared to the grains.

In core samples, the first-generation calcite crystals (Cal1S) are free of, or very poor in, Mn and Fe. The second-generation crystals (Cal2S) have variable Mn and Fe content. In core samples, $FeCO_3$ varies between 0 and 1.9 %, $MnCO_3$ between 0 and 0.5%, and $MgCO_3$ between 0.3 and 2.4%. In outcrop samples, dull red luminescent calcite (Cal2K) stains blue and it is Fe-rich, while, mauve-stained calcite of bright orange luminescent colour (Cal3K) is Mn-rich. $FeCO_3$ content of calcite varies between 0.5 and 2.8 %, whereas that of $MnCO_3$ is between 0.3 and 1.6 %. The $MgCO_3$ content of the calcite in outcrop samples is below 0.8 %; however, the majority of the calcite does not contain measurable Mg. It was not possible to measure Cal1K due to its small size.

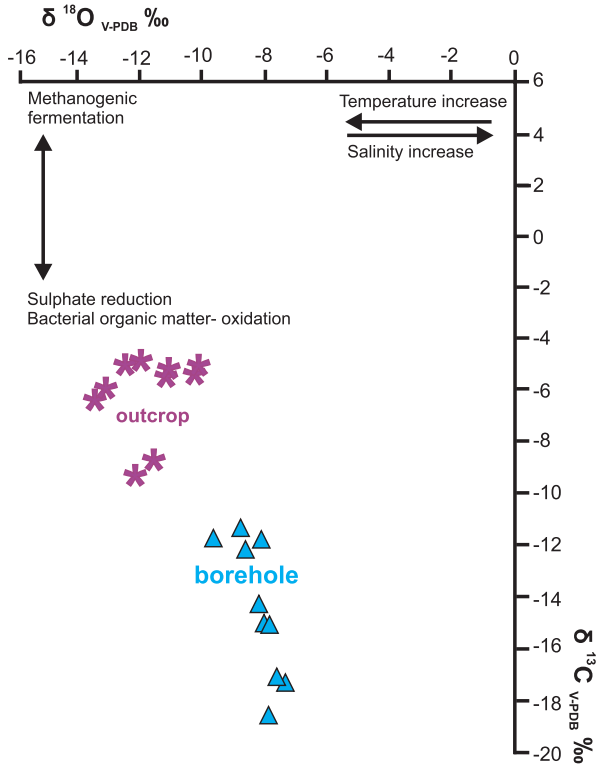

Fig. 8. Cross-plot of the stable isotope values of the studied calcite. Arrows show the influence of methanogenic fermentation, bacterial sulphate reduction, salinity and temperature after (Allan & Wiggins 1993).

Discussion

Paragenetic sequence

Based on petrographic and geochemical observations the paragenetic sequence was established (Fig. 9). Diagenetic realms are adapted from the model by Morad et al. (2000).

Eogenesis and early mesogenesis

The early diagenetic components are recognised in terms of their relation to mechanical compaction.

Interpretation of peculiar calcite phases

In the outcrop section, where Cal1K is present, point-contacts are characteristic; otherwise, linear contacts occur. Since

the Cal3K phase occurs in crystallographic continuity with non-luminescent Cal1K, the latter is interpreted as replacement of a precursor carbonate cement. The compactional features of the grains and the textural relationship of the crystals suggest that the precursor phase of Cal1K was precipitated during an early stage of diagenesis, and was replaced by Cal3K during mesogenesis.

In core section (LF3), calcite cement (Ca1S) can also be inferred as pre-compactional from point contacts and linear contacts of neighbouring grains.

Other components

These components are similar in core and outcrop sections. In the studied samples, glauconite formed in the intragranular pores of bioclasts during early marine diagenesis by a bacterially catalysed process likely similar to what was described by Odin & Matter (1981). In matrix-rich sandstone, framboidal pyrite was precipitated via the alteration processes of organic matter in the zone of bacterial sulphate reduction, likely during the early stage of diagenesis (e.g., Berner et al. 1985). Early calcite phases and siderite were precipitated in the primary pore space, indicating eogenetic origin. Later on, illitisation of smectite as well as albitisation of K-feldspar and plagioclase occurred in the studied sandstone, as discussed by (Land & Milliken 1981) in the Oligocene Frio Formation.

Late mesogenesis in core section

In the core section, ankerite and albite formation pre-dated calcite (Cal2S), since ankerite and albite crystals are engulfed by Cal2S spars. Quartz cement is only present in calcite-free intervals (LF1, LF2), which indicates that quartz formation post-dated that of calcite. Later on, kaolinite replaced the feldspar grains and partial dissolution of feldspars led to formation of secondary intragranular porosity. The amount of secondary porosity and kaolinite is much higher in LF1 and LF2, suggesting that diagenetic calcite hindered this process. In LF1 and LF2 a micron-sized calcite phase (Cal3S), present in small quantities in the euhedral surfaces of kaolinite and quartz, is the latest diagenetic mineral.

Late mesogenesis and telogenesis in outcrop section

In the outcrop section, quartz cement precipitation, formation of the kaolinite via feldspar replacement and secondary porosity were widespread in LF1, LF2 and LF3. These processes were post-dated by the volumetrically significant calcite formation (Cal2K and Cal3K) in LF3. As K-feldspar cementation occurs only in calcite-free sandstone (LF, LF2), this suggests that K-feldspar cementation probably post-dated calcite cementation.

Origin and sources of diagenetic carbonates

Siderite

Siderite is one of the earliest diagenetic carbonate forms present in each lithofacies in both core and outcrop section. Substitution of Mg and Ca for Fe in crystals suggests marine pore-waters and eogenetic precipitation (Mozley 1989).

The penecontemporaneous formation of siderite and pyrite was documented by several studies (Pye et al. 1990; Moore et al. 1992; Karim et al. 2010). Pyrite formation could occur in a bacterial sulphate reduction zone. Formation of iron-sulphide in small amounts in these environments allows the increase of Fe^{2+}, necessary for siderite formation (Morad 1998). The formation of siderite requires reducing, non-sulphidic pore-waters, usually evolving in suboxic and microbial

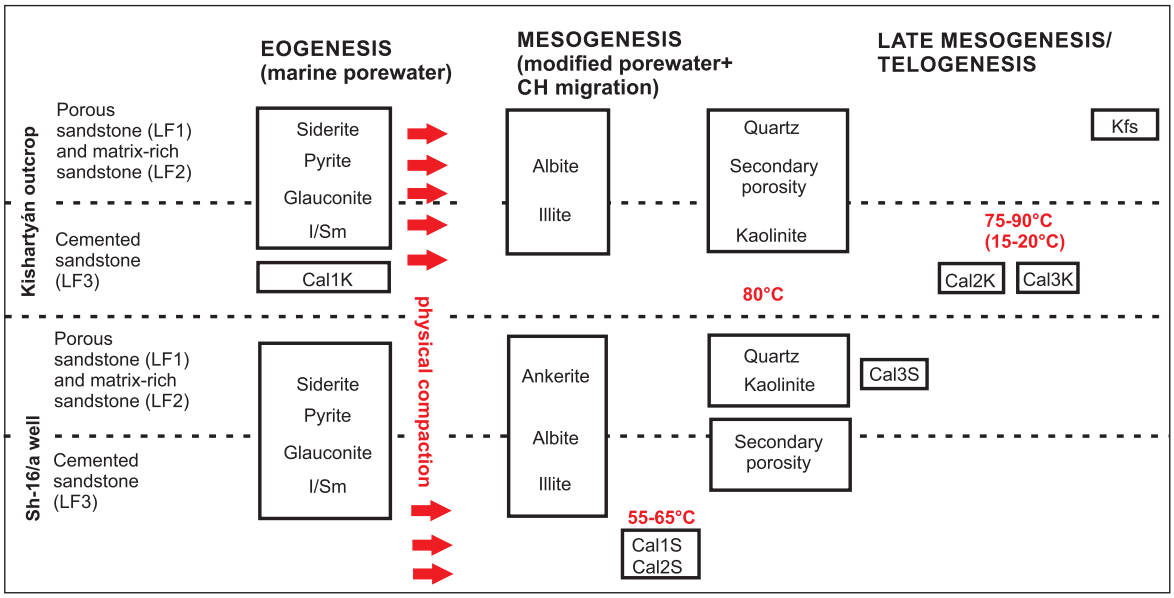

Fig. 9. Paragenetic sequence.

methanogenetic zones (Morad 1998). Fe in siderite usually originates from alteration of iron rich detrital minerals (Zhang et al. 2001).

Ankerite — core section

Ankerite formation in sandstone was documented in association with thermal decarboxylation of organic matter (Kantorowicz 1985; Calvo et al. 2011; Khalifa et al. 2017) where the Mg originated from clay mineral transformations (e.g., Hendry 2002). In the studied sandstone, the chemical heterogeneity which was observed in the composition of ankerite reflects the geochemistry of both pore-water and precursor siderite mineral phase (Fig. 6E,F). Diagenetic reactions in neighbouring lithologic units can be a possible extrernal source of ankerite through cross-formational fluid flow.

Calcite — core section

The calculated precipitation temperature of calcite is 55–65 °C, based on the measured oxygen isotope values (Cal1S and Cal2S), using the oxygen isotopic composition of Early Miocene sea water of the Central Paratethys (Abreu & Anderson 1998) and the oxygen isotope fractionation factor of calcite-water (Friedman & O'Neil 1977). The measured $\delta^{13}C_{V\text{-}PDB}$ data show strong negative values (−18,3 to −11,4 ‰), which indicate an addition of isotopically light carbon from an organic source. Isotopically light carbon was likely released during thermal decarboxylation of organic matter, since the calculated temperature corresponds to that process (cf. Lonoy et al. 1986; Wang et al. 2016). This is in accordance with the presence of residual organic matter as mineral cement covering the calcite crystals. Accordingly, only a minor amount of hydrocarbons migrated from underlying shales after thermal maturation. Grundtner et al. (2017) reported similar isotopic values in calcite cement of Upper Eocene sandstone from the North Alpine Foreland Basin (Austria) and concluded that cementation occurred during advanced stage of sulphate reduction. The possible source of Mg in this calcite can be the ankerite which was replaced by these calcite phases. Ankerite filled hairline fractures of compactional origin in dolomite grains in calcite-free sandstone (LF1, LF2), and the lack of this phenomenon in cemented sandstone (LF3) indicates that uneven calcite cement (Cal1S) was precipitated in primary pore space prior to the compaction.

Micron-sized calcite plates (Cal3S) post-date kaolinite and secondary porosity on feldspar and occur only in calcite-free intervals (LF1, LF2). This represents the latest diagenetic event that differs from the previous calcite-precipitating stages. Considering that the chemistry of present-day pore-water is characteristic for evolved meteoric waters, the rock-water interaction likely resulted in dissolution of unstable minerals, and precipitation of minor calcite cement (Cal3S) (Yuan et al. 2017; Wang et al. 2018).

Calcite — outcrop section

Volumetrically significant calcite phases (Cal2K, Cal3K) post-date quartz cementation in the outcrop section. As reported by McKinley et al. (2002), quartz formation generally requires a minimum temperature of 80 °C, suggesting that in calcite, formation occurred after the sandstone reached the burial depth necessary for this temperature. The measured oxygen isotope values of calcite are enriched in light isotope. These data suggest precipitation either from formation water of elevated temperature or from meteoric water. In the first case, the calculated formation temperature is 75–90 °C, by using the equation of Friedman & O'Neil (1977) and considering isotopic values of Early Miocene sea water of Central Paratethys (Abreu & Anderson 1998). In the second case, the calculated temperature of calcite formation is 15–20 °C, where isotope values of Pleistocene meteoric water are taken into account for comparison (Siklósy et al. 2011; Virág et al. 2013). Carbon isotopic values (from −9,9 to −5,1 ‰) are less enriched in light isotopes compared to the core samples. Source rocks in the underlying formation are present in limited quantity, and their thickness increases toward the cored section (Kázmér 2004; Badics & Vető 2012). This can explain a smaller contribution of light isotope from the organic source. A comparable carbon isotopic ratio can occur in the case of meteoric water recharge, when the light carbon was derived from the soil zone through decay of plant remnants (e.g., El-ghali et al. 2006). Accordingly, in the case of the outcrop section, two possible scenarios can be described for the origin of Ca12K and Cal3K calcites. These volumetrically significant calcite phases were either precipitated in the mesogenetic realm from a formational fluid enriched in light isotopes through organic matter maturation, or in the telogenetic zone from meteoric water recharge during basin inversion.

The studied sandstone is relatively poor (<2 %) in bioclast and limestone rock fragments; tightly calcite-cemented zones are not restricted to layers with abundant fossils or carbonate rock fragments (cf. Grundtner et al. 2016). These indicate that such grains cannot be considered as an internal source for diagenetic calcite. Other possible internal source of calcite can be feldspar dissolution and clay mineral transformations (Dutton 2008). The relatively high quantity of diagenetic calcite suggests an external source, which could be the underlying calcareous marl or overlying bioclastic limestone.

Origin and sources of other diagenetic minerals

The distribution and petrographic features of diagenetic minerals, except for carbonates, are very similar in each lithofacies of the core and outcrop sections. The diagenetic realms and origin of these minerals were interpreted based on literature data.

In the realm of mesogenesis the partial albitisation of detrital feldspar and illitisation of smectites were widespread in both sections (cf. Saigal et al. 1988; Aagaard et al. 1990). Given the similar quantity of diagenetic albite, quartz, and

illite in the studied sandstone, the sources of ions for these reactions were most likely internal or from the clay-rich layers of the sandstone. Post-compactional K-feldspar overgrowth cement, present only in the outcrop section, could have been precipitated from evolved meteoric water at near-surface p/T condition. K^+ was possibly sourced from the alteration of clay minerals (Morad et al. 1989; Maraschin et al. 2004). Diagenetic kaolinite was probably sourced from the weathering of feldspars (Marfil et al. 2003; Waldmann & Gaupp 2016; Yuan et al. 2017)

Thermal history and fluid flow

Core section

Limited pore-water data available from the Sh-16/a core section suggest a complex hydrogeologic system. Elevated temperature values (68 °C at 1100 m) in calcareous marls, directly underlying the Pétervására Sandstone, are characteristic for the formation water of those deposits which were affected by the high heat flow in the Pannonian Basin (95 mW/m^2; Lenkey et al. 2001). High heat-flow values originated from the Middle Miocene extension and thinning of the lithosphere (Royden & Baldi 1988). Accordingly, the fluid originating from the underlying formation could have been the source of calcite cement. Moreover, together with these fluids, minor hydrocarbons also migrated from marls. Significant negative shift of carbon isotopic values of calcite, and additionally the residual bitumen on crystal surfaces, suggest that calcite was precipitated from formation fluids connected to organic matter maturation.

The present day pore-water of the studied sandstone in the core section at ~880 m has a much lower temperature (37 °C) and a composition characteristic for evolved meteoric waters (cf. Yuan et al. 2015). Based on the geodynamic evolution of the basin, the studied sandstone formation was also affected by the high heat flow (Lenkey et al. 2001), but later on was recharged by gravity-driven, regional meteoric flow systems (Tóth & Almasi 2001; Horváth et al. 2015). The evolved meteoric fluid is likely responsible for dissolution and kaolinite formation. Micron-sized calcite plates (Cal3S) could also have been precipitated from the meteoric fluid.

Outcrop section

The studied section is located at the proximity of a large-scale normal fault, in a hanging wall setting (Püspöki et al. 2017). The diagenetic minerals association suggests that calcite cementation (Cal2K, Cal3K) post-dated quartz cementation, which approximately took place when the Pétervására Sandstone reached its maximum burial depth around 8–11 Ma (Petrik et al. 2014; Beke 2016). Accordingly, calcite cementation either occurred during late mesogenesis (75–90 °C), or later on, in relation to uplift and telogenesis (15–20 °C). During basin inversion, progressive recharge of meteoric water led to the precipitation of telogenetic minerals such as K-feldspar.

Conclusions

- The diagenetic history of the Lower Miocene Pétervására Sandstone in outcrop and borehole setting was reconstructed.
- In litharenite and feldspathic litharenite, the most significant eogenetic minerals, precipitated in a marine environment, are siderite, calcite, pyrite; the mesogenetic minerals are replacive albite, ankerite, calcite, quartz, mixed layer clays and kaolinite. Minerals of telogenetic origin are kaolinite, K-feldspar and possibly a minor amount of calcite.
- Mesogenetic ankerite occurs only in the core section, whereas telogenetic K-feldspar is characteristic solely for the outcrop section.
- The geochemical composition of diagenetic carbonate minerals shows a wide variability. Elemental composition of siderite is characteristic for marine pore-water. Calcite in core samples is relatively enriched in $MgCO_3$, probably due to replacement of ankerite.
- In the core section, sandstone is at ca. 900 m depth and diagenetic calcite pre-dates quartz cementation. Based on stable isotopic values ($\delta^{13} C_{V\text{-}PDB}$ −18.3 to −11.4 ‰ and $\delta^{18} O_{V\text{-}PDB}$ −9.5 to −7.2 ‰) the diagenetic calcite is of mesogenetic origin and was precipitated from fluids migrated along fault zones from the underlying, organic matter-rich formation. The formation temperature calculated for calcite is of 55–65 °C.
- In the outcrop setting, the calcite is present in larger quantity and post-dates quartz cementation. Carbon isotope data ($\delta^{13} C_{V\text{-}PDB}$=−9.9 to −5.1 ‰) indicate less contribution of light isotopes, whereas more negative oxygen isotopic values ($O_{V\text{-}PDB}$=−13.1 to −9.9 ‰) likely indicates a higher temperature of mesogenetic fluids. However, carbon-oxygen isotope covariation can point to precipitation from a meteoric fluid.
- Additionally, a minor amount of calcite of likely eogenetic origin was observed in the outcrop section; telogenetic calcite precipitation connected to modified meteoric pore fluids was observed in the core section.

Acknowledgements: This paper is based on the MSc thesis of E. Szőcs. We are grateful to Attila Demény for stable isotopic measurements, to Tibor Németh for clay mineralogical analysis and to Tomáš Mikuš for electron microanalysis. Orsolya Sztanó, Barbara Beke, László Fodor, Sándor Józsa, Zsolt Bendő, Gergely Surányi, Orsolya Győri, Andrea Mindszenty, Zsófia Poros, Balázs Szinger, István Vető, Szilvia Simon and Miklós Varga are acknowledged for the discussion on the topic and their help in field work. The cores were provided by the core sample storage of the Hungarian Office for Mining and Geology in cooperation with the Geological and Geophysical Institute of Hungary. The project was partially supported through the New National Excellence Program of the Ministry of Human Capacities, Hungary (ÚNKP-17 to E. Szőcs). The authors appreciate the constructive comments and suggestions

of anonymous Referees, Handling Editor and Managing Editor. The authors are grateful to Henry Lieberman for English grammar correction.

References

Aagaard P., Egeberg Z.P.K., Saigal G.C., Morad S. & Bjorlykke K. 1990: Diagenetic albitization of detrital K-feldspars in Jurassic, Lower Cretaceous and Tertiary clastic reservoir rocks from offshore Norway, II. Formation water chemistry and kinetic considerations. *J. Sediment. Petrol.* 60, 575–581.

Abreu V.S. & Anderson J.B. 1998: Glacial eustasy during the Cenozoic: sequence stratigraphic implications. *Am. Assoc. Pet. Geol. Bull.* 82, 1385–1400.

Allan J.R. & Wiggins W.D. 1993: Dolomite reservoirs: Geochemical Techniques for Evaluating Origin and Distribution. *American Association of Petroleum Geologists Continuing Education Course Note Series*, Tulsa, Oklahoma, 1–170.

Badics B. & Vető I. 2012: Source rocks and petroleum systems in the Hungarian part of the Pannonian Basin: The potential for shale gas and shale oil plays. *Mar. Pet. Geol.* 31, 53–69.

Baker J.C., Kassan J. & Hamilton P.J.O.E. 1995: Early Diagenetic Siderite as an Indicator of Depositional Environment in the Triassic Rewan Group, Southern Bowen Basin, Eastern Australia. *Sedimentology* 43, 77–88.

Báldi T. 1983: The Oligocene and Lower Miocene formations of Hungary. *Akadémiai Kiadó*, Budapest, 1–293 (in Hungarian).

Báldi T. & Báldi-Beke M. 1985: The evolution of the Hungarian Paleogene basins. *Acta Geol. Hungarica*. 28, 5–28 (in Hungarian).

Beke B.K. 2016: The role of deformation bands in Cenozoic structural evolution of Northern Hungary, PhD thesis. *Eötvös Loránd University*, Budapest, 1–148 (in Hungarian).

Berner, R. A., Leeuw J.W. De, Spiro B., Murchison D.G. & Eglinton G. 1985: Sulphate Reduction, Organic Matter Decomposition and Pyrite Formation. *Philos. Trans. R. Soc. London. Ser. A, Math. Phys. Sci*. 315, 25–38.

Bojanowski M.J., Barczuk A. & Wetzel A. 2014: Deep-burial alteration of early-diagenetic carbonate concretions formed in Palaeozoic deep-marine greywackes and mudstones (Bardo Unit, Sudetes Mountains, Poland). *Sedimentology.* 61, 1211–1239.

Calvo R., Ayalon A., Bein A. & Sass E. 2011: Chemical and isotopic composition of diagenetic carbonate cements and its relation to hydrocarbon accumulation in the Heletz-Kokhav oil field (Israel). *J. Geochemical Explor.* 108, 88–98.

Dickson J. 1966: Carbonate identification and genesis as revealed by staining. *J. Sediment. Petrol.* 36, 491–505.

Dutton S.P. 2008: Calcite cement in Permian deep-water sandstones, Delaware Basin, west Texas: Origin, distribution, and effect on reservoir properties. *Am. Assoc. Pet. Geol. Bull.* 92, 765–787.

El-ghali M.A.K., Tajori K.G., Mansurbeg H., Ogle N. & Kalin R.M. 2006: Origin and timing of siderite cementation in Upper Ordovician glaciogenic sandstones from the Murzuq basin, SW Libya. *Mar. Pet. Geol.* 23, 459–471.

Folk R.L. 1974: Petrology of sedimentary rocks. *Hemphill Publishing Company*. Austin, Texas, 1–190.

Friedman I. & O'Neil J. 1977: Compilation of Stable Isotope Fractionation Factors of Geochemical Interest. In: M. Fleischer (Ed.): Data of Geochemistry. *US Geological Survey Professional Paper*, 440-KK, Washington.

Gier S., Worden R.H., Johns W.D. & Kurzweil H. 2008: Diagenesis and reservoir quality of Miocene sandstones in the Vienna Basin, Austria. *Mar. Pet. Geol*. 25, 681–695.

Gradstein F. & Ogg J. 2004: Geologic Time Scale 2004 — why, how, and where next!. *Lethaia* 37, 175–181.

Grundtner M.L., Gross D., Gratzer R., Misch D., Sachsenhofer R.F. & Scheucher L. 2017: Carbonate cementation in upper eocene clastic reservoir rocks from the north alpine foreland basin (Austria). *Austrian J. Earth Sci*. 110, 55–75.

Grundtner M.L., Gross D., Linzer H.G., Neuhuber S., Sachsenhofer R.F. & Scheucher L. 2016: The diagenetic history of Oligocene-Miocene sandstones of the Austrian north Alpine foreland basin. *Mar. Pet. Geol*. 77, 418–434.

Hámor T. 1985: Geological report on Sámsonháza- 16/a well. *Geological Institute of Hungary*, Budapest, 1–16,

Hendry J.P. 2002: Geochemical trends and palaeohydrological significance of shallow burial calcite and ankerite cements in Middle Jurassic strata on the East Midlands Shelf (onshore UK). *Sediment. Geol*. 151, 149–176.

Hendry J.P., Wilkinson M., Fallick A.E. & Haszeldine R.S. 2000: Ankerite cementation in deeply buried Jurassic sandstone reservoirs of the central North Sea. *J. Sediment. Res*. 70, 227–239.

Horváth F. & Tari G. 1999: IBS Pannonian Basin project: a review of the main results and their bearings on hydrocarbon exploration. *Geol. Soc. London*, Spec. Publ. 156, 195–213.

Horváth F., Musitz B., Balázs A., Végh A., Uhrin A., Nádor A. & Koroknai B. 2015: Geothermics Evolution of the Pannonian basin and its geothermal resources. *Geothermics* 53, 328–352.

Kantorowicz J.D. 1985: The origin of authigenic ankerite from the Ninian Field, UK North Sea. *Nature* 315, 214–216.

Karim A., Pe-Piper G. & Piper D.J.W. 2010: Controls on diagenesis of Lower Cretaceous reservoir sandstones in the western Sable Subbasin, offshore Nova Scotia. *Sediment. Geol.* 224, 65–83.

Kázmér M. 2004: Hydrocarbon geology o f northem Hungary (Palaeogene basin), in: Kázmér, M. (Ed.), General Geological Review Journal of the Section for General Geology Hungarian Geological Society. *Hantken Kiadó*, Budapest, 9–120.

Khalifa M.A., Mansurbeg H., Morad D., Morad S., Al-Aasm I.S., Spirov P., Ceriani A. & De Ros L.F. 2017: Quartz and Fe-dolomite Cements Record Shifts in Formation-water Chemistry and Hydrocarbon Migration in Devonian Shoreface Sandstones, Ghadamis Basin, Libya. J. *Sediment. Res*. 88, 38–57.

Lakatos L., Varadi M., Pogacsas G., Nagymarosy A., Kis B. & Barvitz A. 1991: Sequence stratigraphy of Paleogene Formations in Zagyva Trough. *Hung. Geophys*. 20–37 (in Hungarian).

Land L.S. & Milliken K.L. 1981: Feldspar diagenesis in the Frio formation, Brazoira County, Texas Gulf Coast. *Geology* 9, 314–318.

Lenkey L., Dövényi P., Horváth F. & Cloetingh S. a. P.L. 2001: Geothermics of the Pannonian basin and its bearing on the neotectonics. *EGU Stephan Mueller Spec. Publ. Ser*. 3, 29–40.

Lima R.D. & De Ros L.F. 2002: The role of depositional setting and diagenesis on the reservoir quality of Devonian sandstones from the Solimões Basin, Brazilian Amazonia. *Mar. Pet. Geol.* 19, 1047–1071.

Lonoy A., Akselsen J. & Ronning K. 1986: Diagenesis of a deeply buried sandstone reservoir; Hild Field, northern North Sea. *Clay Miner*. 497–511.

Makeen Y.M., Abdullah W.H., Ayinla A.A., Hakimi M.H. & Sia S.G. 2016: Sedimentology, diagenesis and reservoir quality of the upper Abu Gabra Formation sandstones in the Fula Sub-basin, Muglad Basin, Sudan. *Mar. Pet. Geol.* 77, 1227–1242.

Maraschin A.J., Mizusaki A.M.P. & De Ros L.F. 2004: Near-Surface K-Feldspar Precipitation in Cretaceous Sandstones from the Potiguar Basin, Northeastern Brazil. *J. Geol.* 112, 317–334.

Marfil R., Delgado A., Rossi C., La Iglesia A. & Ramseyer K. 2003: Origin and diagenetic evolution of kaolin in reservoir sandstones and associated shales of the Jurassic and Cretaceous, Salam Field, Western Desert (Egypt). In: Worden, R.H., Morad, S. (Eds.): Sandstone Diagenesis: The Evolution of Sand to Stone.

International Association of Sedimentologists, Bodmin, Cornwall. 319–342.

Márton E. & Fodor L. 1995: Combination of palaeomagnetic and stress data: a case study from Northern Hungary. *Tectonophysics* 242, 99–114.

McBride E.F., Milliken K., Cavazza W., Cibin U., Fontana D., Picard M.D. & Zuffa G.G. 1994: Patterns of calcite cementation at the outcrop scale in Tertiary sandstones. *AAPG Annu. Conv*. 1–209.

McKinley J.M., Worden R.H. & Ruffell a H. 2002: Smectite in sandstones: A review of the controls on occurrence and behaviour during diagenesis. *Int. Assoc. Sedimentol. Spec. Publ.* 109–128.

Milota K., Kovacs A. & Galicz Z. 1995: Petroleum potential of the North Hungarian Oligocene sediments. *Pet. Geosci*. 1, 81–87.

Moore S.E., Ferrell R.E. & Aharon P. 1992: Diagenetic siderite and other ferroan carbonates in a modem subsiding marsh sequence. *J. Sediment. Petrol*. 62, 357–366.

Morad S. 1998: Carbonate Cementation in Sandstones: Distribution Patterns and Geochemical Evolution. In: Morad S. (Ed.): Carbonate Cementation in Sandstones: Distribution Patterns and Geochemical Evolution. *Special Publication 26 of the IAS*, *University Press*, Cambridge, 1–26.

Morad S., Márfil R. & Pena J. 1989: Diagenetic K-feldspar pseudomorphs in the Triassic Buntsandstein sandstones of the Iberian Range, Spain. *Sedimentology* 36, 635–650.

Morad S., Ketzer J.M. & De Ros L.F. 2000: Spatial and temporal distribution of diagenetic alterations in siliciclastic rocks: Implications for mass transfer in sedimentary basins. *Sedimentology* 47, 95–120.

Mozley P.S. 1989: Relation between depositional environment and the elemental composition of early diagenetic siderite. *Geology* 17, 704–706.

Nagymarosy A. 2012: Accretion of the ALCAPA Mega-Unit. In: Haas J., Hámor G., Jámbor Á., Kovács S., Nagymarosy A. & Szederkényi T. (Eds.): Geology of Hungary. *Springer-Verlag*, Berlin Heidelberg, 81–102.

Nickel E.H. & Grice J.D. 1998: The IMA Commission on New Minerals and Mineral Names: procedures and guidelines on mineral nomenclature, 1998. *Can. Mineral.* 36, 1–14.

Odin G. & Matter A. 1981: De glauconiarum origine. *Sedimentology* 28, 611–641.

Oluwadebi A.G., Taylor K.G. & Dowey P.J. 2018: Diagenetic controls on the reservoir quality of the tight gas Collyhurst Sandstone Formation, Lower Permian, East Irish Sea Basin, United Kingdom. *Sediment. Geol*. 371, 55–74.

Petrik A., Beke B. & Fodor L. 2014: Combined analysis of faults and deformation bands reveals the Cenozoic structural evolution of the southern Bükk foreland (Hungary). *Tectonophysics* 633, 43–62.

Püspöki Z., Hámor-Vidó M., Pummer T., Sári K., Lendvay P., Selmeczi I., Detzky G., Gúthy T., Kiss J., Kovács Z., Prakfalvi P., McIntosh R.W., Buday-Bódi E., Báldi K. & Markos G. 2017: A sequence stratigraphic investigation of a Miocene formation supported by coal seam quality parameters — Central Paratethys, N-Hungary. *Int. J. Coal Geol*. 179, 196–210.

Pye K., Dickson J., Schiavon N., Coleman M.L. & Cox M. 1990: Formation of siderite-Mg-calcite-iron sulphide concretions in intertidal marsh and sandflat sediments, north Norfolk, England. *Sedimentology* 37, 325–343.

Rögl F. & Steininger F.F. 1983: Vom Zerfall der Tethys zu Mediterran und Paratethys. Wien. *Ann. Naturhistorische Museum* 85, 135–163.

Royden L. & Baldi T. 1988: Early Cenozoic tectonics and paleogeography of the Pannonian basin and surrounding regions. In: Royden L.R., Horvath F. (Eds.): The Pannonian Basin a Study in Basin Evolution. *Amer. Assoc. Petro Geol.*, Memoir 45, 1–16.

Saigal G.C.G., Morad S., Bjorlykke K., Egeberg P.K. & Aagaard P. 1988: Diagenetic albitization of detrital K-feldspar in Jurassic, Lower Cretaceous, and Tertiary clastic reservoir rocks from offshore Norway; I, Textures and origin. *J. Sediment. Petrol*. 58, 1003–1013.

Siklósy Z., Demény A., Leél-Őssy S., Szenthe I., Lauritzen S.-E. & Shen C. 2011: The dating of stalagmites and their palaeoclimatological significance. *Bull. Hungarian Geol. Soc.* 141, 73–88.

Szőcs E., Hips K., Józsa S. & Bendő Z. 2015: Diagenetic evolution of the Lower Miocene Pétervására Sandstone Formation. *Bull. Hung. Geol. Soc.* 145, 351–366 (in Hungarian).

Sztanó O. 1994: The tide-influenced Petervasara Sandstone, early Miocene, northern Hungary: sedimentology, palaeogeography and basin development. *Geol. Ultraiectina,* Uthrecht, 120, 155.

Sztanó O. & Boer P. 1995: Basin dimensions and morphology as controls on amplification of tidal motions (the Early Miocene North Hungarian Bay). *Sedimentology* 42, 665–682.

Sztanó O. & Józsa S. 1996: Interaction of basin-margin faults and tidal currents on nearshore sedimentary architecture and composition: a case study from the Early Miocene of northern Hungary. *Tectonophysics* 266, 319–341.

Sztanó O. & Tari G. 1993: Early Miocene basin evolution in Northern Hungary: tectonics and eustasy. *Tectonophysics* 261, 485–502.

Tari G., Báldi T. & Báldi-Beke M. 1993: Paleogene retroarc flexural basin beneath the Neogene Pannonian Basin: a geodynamic model. *Tectonophysics* 226, 433–455.

Tóth J. & Almasi I. 2001: Interpretation of observed fluid potential patterns in a deep sedimentary basin under tectonic compression: Hungarian Great Plain, Pannonian Basin. *Geofluids* 1, 11–36.

Van Den Bril K. & Swennen R. 2008: Sedimentological control on carbonate cementation in the Luxembourg Sandstone Formation. *Geol. Belgica* 12, 3–23.

Virág M., Mindszenty A., Surányi G., Molnár M. & Leél-Őssy S. 2013: A Búboskemence cseppkőlefolyás. In: Mindszenty A. (Ed.): Budapest Földtani Értékek És Az Ember. Városgeológiai Tanulmányok. *ELTE Eötvös Kiadó*, Budapest, 245–248 (in Hungarian*)*.

Waldmann S. & Gaupp R. 2016: Grain-rimming kaolinite in Permian Rotliegend reservoir rocks. *Sediment. Geol*. 335, 17–33.

Wanas H.A. 2008: Calcite-cemented concretions in shallow marine and fluvial sandstones of the Birket Qarun Formation (Late Eocene), El-Faiyum depression, Egypt: Field, petrographic and geochemical studies: Implications for formation conditions. *Sediment. Geol*. 212, 40–48.

Wang J., Cao Y., Liu K., Liu J., Xue X. & Xu Q. 2016: Pore fluid evolution, distribution and water-rock interactions of carbonate cements in red-bed sandstone reservoirs in the Dongying Depression, China. *Mar. Pet. Geol*. 72, 279–294.

Wang J., Cao Y., Liu K., Costanzo A. & Feely M. 2018: Diagenesis and evolution of the lower Eocene red-bed sandstone reservoirs in the Dongying Depression, China. *Mar. Pet. Geol.* 94, 230–245.

Yuan G., Cao Y., Cluyas J., Li X., Xi K., Wang Y., Jia Z., Sun P. & Oxtoby N.H. 2015: Feldspar dissolution, authigenic clays, and quartz cements in open and closed sandstone geochemical systems during diagenesis: Typical examples from two sags in Bohai Bay Basin, East China. *Am. Assoc. Pet. Geol. Bull*. 99, 2121–2154.

Yuan G., Cao Y., Zhang Y. & Gluyas J. 2017: Diagenesis and reservoir quality of sandstones with ancient "deep" incursion of meteoric freshwater —An example in the Nanpu Sag, Bohai Bay Basin, East China. *Mar. Pet. Geol*. 82, 444–464.

Zhang C.L., Horita J., Cole D.R., Zhou J., Lovley D.R. & Phelps T.J. 2001: Temperaturedependent oxygen and carbon isotope fractionation of biogenic siderite. *Geochim. Cosmochim. Acta* 65, 2257–2271.

Supplement

Appendix 1: Quantitative composition of sandstone according to point counting (%).

		samples from outcrop															samples from core		
lithofacies		LF1 porous sandstone						LF2 matrix-rich sandstone			LF3 cement-rich sandstone						LF3	LF2	LF1
sample		B-7/c	B-11/a	D-20	A-3	B-10/a	B-11/b	B-9/b	A-2	B-13/e	A-4	B-13/c	A-5	B-12/b	B-14/c	B-10/b	988m	903m	873m
grains	quartz+ chert	31	36	37	36	43	37	28	29	35	23	28	27	29	37	36	33	30	33
	feldspar	8	6	7				8			9	4	8	9			6	5	5
	magmatic + metamorphic rock fragment	11	13	20	20	20	39	13	11	21	31	20	26	29	30	22	16	28	30
	volcanic rock fragment	12	12	7	13	18	10	7	10	4	6	7	1	4	5	9	1	1	1
	bioclast								<1		<1				<1		2		
	iron oxide	5	4	3	3			5	4	2		1	2	<1	1	1	1		
	dolomite	4	3	6	7	2	3	4	4	8	2	9	9	6	5	4	12	10	11
matrix	matrix		2	1	9	4		28	19	13	1			1		6	0	18	4
cement	calcite					2		1	14	10	23	18	17	16	7	7	11		
	replacive calcite					1			8	2	5	4	1	4	3	2	17		
	siderite	4	4	1	3	2	3	1	1			3	4	3	2	1	2	3	6
pores	intergranular	20	17	17	8	8	8	3	1	4	<1	5	4	<1	8	8		4	7
	intragranular	5	3	1	2	1	1	2	1	1		1	1		2	2		2	4

Appendix 2: Chemical composition of diagenetic carbonate minerals in the Pétervására Sandstone.

Sample number	Mineral	$CaCO_3$ %	$MnCO_3$ %	$MgCO_3$ %	$FeCO_3$ %	$SrCO_3$ %	CO_2 (Mass %)	Total (Mass %)
core sample 988	calcite	98.54	0.08	0.65	1.93	0.10	44.72	101.73
core sample 988	calcite	98.35	0.30	1.39	0.03	0.00	44.20	100.26
core sample 988	calcite	100.38	0.12	0.43	1.79	0.15	45.15	102.91
core sample 988	calcite	100.73	0.22	0.88	0.11	0.06	44.93	102.06
core sample 988	calcite	98.79	0.30	1.23	0.01	0.00	44.23	100.37
core sample 988	calcite	99.57	0.14	0.34	1.35	0.02	44.55	101.45
core sample 988	calcite	99.93	0.16	1.65	0.01	0.04	44.89	101.83
core sample 988	calcite	95.23	0.03	1.40	0.08	0.09	43.07	97.50
core sample 988	calcite	99.54	0.26	0.74	0.02	0.03	44.32	100.66
core sample 988	calcite	98.01	0.23	1.33	0.13	0.00	43.97	99.76
core sample 988	calcite	101.26	0.25	2.22	0.05	0.00	45.79	103.75
core sample 988	calcite	100.03	0.29	1.71	0.00	0.00	45.00	102.04
core sample 988	calcite	99.69	0.27	1.81	0.07	0.00	45.02	102.02
core sample 988	calcite	101.20	0.05	0.88	0.02	0.03	44.97	102.12
core sample 988	calcite	97.49	0.25	2.00	0.03	0.02	44.14	99.98
core sample 988	calcite	100.43	0.27	1.20	0.22	0.07	45.04	102.25
core sample 988	calcite	96.76	0.16	0.64	0.06	0.11	43.03	97.78
core sample 988	calcite	100.01	0.46	1.34	0.28	0.00	45.01	102.20
core sample 988	calcite	100.90	0.14	1.17	0.06	0.04	45.04	102.25
core sample 988	calcite	98.98	0.26	2.44	0.10	0.00	44.92	101.75
core sample 988	calcite	101.56	0.28	1.55	0.09	0.07	45.66	103.58

Appendix 2 (continued): Chemical composition of diagenetic carbonate minerals in the Pétervására Sandstone.

Sample number	Mineral	$CaCO_3$ %	$MnCO_3$ %	$MgCO_3$ %	$FeCO_3$ %	$SrCO_3$ %	CO_2 (Mass %)	Total (Mass %)
outcrop sample PB5b	calcite	98.90	1.11	0.37	0.65	0.05	44.39	101.12
outcrop sample PB5b	calcite	98.59	1.31	0.34	0.64	0.01	44.25	100.84
outcrop sample PB5b	calcite	99.13	1.28	0.62	0.97	0.00	44.80	102.04
outcrop sample PB5b	calcite	95.33	1.20	0.39	0.72	0.01	42.87	97.67
outcrop sample PB5b	calcite	97.12	1.28	0.69	1.08	0.05	43.99	100.25
outcrop sample PB5b	calcite	99.30	0.99	0.29	0.63	0.03	44.44	101.24
outcrop sample PB5b	calcite	95.65	1.52	0.67	1.00	0.00	43.44	98.96
outcrop sample PB5b	calcite	97.22	1.63	0.66	0.98	0.02	44.13	100.56
outcrop sample PB5b	calcite	97.66	1.25	0.39	0.91	0.00	44.00	100.27
outcrop sample PB5b	calcite	95.88	1.26	0.73	0.98	0.03	43.41	98.88
outcrop sample PB5b	calcite	97.69	1.23	0.37	0.76	0.00	43.97	100.14
outcrop sample PB5b	calcite	96.60	0.49	0.57	1.31	0.18	43.57	99.23
outcrop sample PB5b	calcite	96.34	1.12	0.31	0.55	0.03	43.19	98.38
outcrop sample PB5b	calcite	97.40	1.22	0.40	0.72	0.04	43.79	99.78
outcrop sample PB5b	calcite	98.95	0.28	0.55	2.78	0.17	45.03	102.77
outcrop sample PB5b	calcite	98.17	1.18	0.44	0.99	0.03	44.25	100.86
988 an 5	ankerite	56.54	0.53	22.35	18.42	0.08	43.75	97.91
988 an 7	ankerite	55.33	0.48	17.39	23.80	0.04	42.71	97.16
core sample 873	ankerite	55.67	0.51	18.82	22.11	0.08	43.00	97.34
core sample 873	ankerite	54.64	0.50	18.46	22.73	0.00	42.62	96.55
core sample 873	siderite	10.82	0.43	10.75	75.43	0.00	39.19	97.45
core sample 873	siderite	10.09	1.29	5.58	80.44	0.03	38.91	98.31
core sample 873	siderite	10.32	0.69	11.25	74.48	0.06	39.02	96.91
core sample 873	siderite	8.72	0.93	15.42	70.92	0.00	39.38	96.40
core sample 873	siderite	11.10	0.35	17.12	68.54	0.04	40.13	97.41
core sample 988	siderite	7.04	0.91	18.75	69.62	0.02	39.72	96.42
core sample 873	siderite	12.08	1.04	11.41	73.66	0.02	40.59	99.85
core sample 873	siderite	8.60	1.26	4.25	81.89	0.00	37.89	96.55
core sample 873	siderite	10.53	1.12	8.07	76.53	0.02	39.35	98.02
core sample 873	ankerite	55.81	0.33	19.29	21.60	0.04	43.03	97.21
core sample 988	dolomite	52.79	0.00	44.69	0.03	0.01	46.48	97.40
core sample 988	dolomite	57.89	0.06	44.31	0.20	0.00	48.64	102.40
outcrop sample PB5b	dolomite	53.80	0.00	45.57	0.27	0.02	47.49	99.54
core sample 873	dolomite	53.99	0.02	43.15	0.80	0.00	46.86	98.43

Appendix 3: Simplified lithostratigraphic chart of the Palaeogene formations in North Hungary (Nagymarosy 2012, modified after Tari et al. 1993).